IEEE Robotics and Automation Letters (RA-L) paper, presented at ICRA 2026, Vienna, Austria. Cite as RA-L paper.

Design and Experimental Validation of a Controller for Bowden-Cable Actuators Subject to Friction Variation

Yaodong Lu, Yannick Aoustin, Pablo Nocito, Sébastien Mick, and Nathanaël Jarrassé

***Abstract*—Exoskeleton robots hold great potential for both industrial applications and assisting patients with locomotor disabilities. Among them, flexible exoskeletons, known as "exosuits", have attracted a great deal of interest from researchers. Those are usually made up of flexible components such as cables and pieces of fabric, which are much lighter than the rigid exoskeletons. By using a Bowden-cable transmission in their design, the actuators can be placed away from the end-effectors of exosuits and thus are considered an effective transmission solution for reducing the weight and inertia felt by operators wearing the exosuit. However, a critical issue of Bowden-cable transmission is the complex and nonlinear friction between the inner cable and outer sheath, which affects the control robustness by introducing a time delay and inaccuracy in position tracking. Besides, friction along the cable varies with the accumulated bending angle of the sheath. A control synthesis approach is proposed for the Bowden-cable actuation system, utilizing twisting and super-twisting algorithms to ensure finite time stability and robustness properties of a perturbed double-integrator model. The experimental results demonstrate the effectiveness of the proposed method across various bending angle conditions.**

***Index Terms*—Bowden-cable transmission, finite time stabilization, nonlinear friction, remote actuation, twisting controller.**

I. Introduction

In THE last decade, exoskeleton robots become one of the potential solutions for assisting the patients with locomotor disability or amplifying physical strength of workers in industrial field [1], [2]. A lot of researches in wearable assistive robotics have led to the development of rigid-frame exoskeletons for applications ranging from patient assistance [3], [4], [5] to strength augmentation for workers [6], [7], [8]. While rigid exoskeletons can deliver high forces and torques, their heavy structure and inertia reduce mechanical transparency, resulting in increased metabolic cost and undesired joint torques for the wearer [9].

Avoiding the drawbacks of rigid exoskeleton, the exoskeleton with flexible structure, named exosuit has aroused great research interest [10], [11], [12]. Unlike the exoskeletons with rigid frames, exosuits are usually fabricated with soft materials like fabrics and cables, and are consequently much lighter. By using a Bowden-cable transmission in exosuit design, the actuators can be placed away from the end-effectors of exosuits and thus are considered an effective transmission solution for reducing the weight and inertia felt by operators wearing the exosuit. In a Bowden-cable transmission, a cable is guided inside a flexible sheath. For remote actuation of a robotic joint, force is delivered to the remote joint by mechanical displacement between the cable and the outer sheath. The Bowden-cable's flexibility leads to its adoption in many exosuit designs that require a transmission path with a complex and varying shape [13], [14], [15], [16]. Typically, in upper limb exoskeletons, the motor is mounted on the user's hip or back, while the driven end-effector is positioned at the elbow or shoulder joint level. As a result, any movement of the trunk, scapula, or shoulder will significantly change the bending angle of Bowden cable, often resulting in variations exceeding 90 degrees.

Despite the many advantages of Bowden-cable transmission applied in the exosuit design, a critical issue of a Bowden-cable is the complex and nonlinear friction between the inner cable and outer sheath [17], which affects the control robustness by introducing a time delay and inaccuracy in position tracking. According to [18], "Friction is the nemesis of precision control". Coulomb friction, viscous friction, stiction and stick-slip, can all occur in Bowden-cable transmission systems. Additionally, friction variation results from changes in the accumulated bending angle of the Bowden cable during operation. This variation can cause the force transmission efficiency to decrease exponentially as the accumulated bending angle increases [19]. In most practical applications of exosuits using Bowden-cable transmission, the relative position between the actuator and the end-effector varies over time when tracking a given trajectory, leading to continuous changes in the bending angles of the sheath. Estimating the friction force under such conditions becomes nearly impossible without specialized sensors capable of measuring the cumulative bending angles of the sheath across its segments [20]. However, to the best of our knowledge, achieving both high measurement accuracy and compatibility with skin or soft fabrics in flexible sensors remains a challenge [21], [22]. The complexity of implementation and the lack of accurate measurements leads

Received 10 March 2025; accepted 8 July 2025. Date of publication 23 July 2025; date of current version 4 August 2025. This article was recommended for publication by Associate Editor A. Sabelhaus and Editor C. Della Santina upon evaluation of the reviewers' comments. This work was supported, in part by JOKER Project (BPI I-démo program of the France 2030 plan), and in part by Reinvent project under Grant ANR-22-EXOD-0002. The work of Yannick Aoustin was supported by ANR project SlimDisc under Grant ANR-24-CE48-2771. *(Corresponding author: Yaodong Lu.)*

Yaodong Lu, Pablo Nocito, Sébastien Mick, and Nathanaël Jarrassé are with Sorbonne Université, CNRS UMR 7222, ISIR, F-75005 Paris, France (e-mail: luy@isir.upmc.fr).

Yannick Aoustin is with ECN-Nantes Université, UMR 6004, LS2N, F-44321 Nantes, France (e-mail: yannick.aoustin@univ-nantes.fr).

This article has supplementary downloadable material available at https://doi.org/10.1109/LRA.2025.3592077, provided by the authors.

Digital Object Identifier 10.1109/LRA.2025.3592077

to unexpected modeling errors and degradation of control performance. Jeong et al. [23] proposed a mechanical solution known as loop routing, which continuously maintains the bending angle at nearly 360°, regardless of the end-effector's position in 2-D space. Although this method allows for accurate feedforward compensation, it also increases overall friction at high bending angles. Hence, it is essential to design an effective control strategy capable of dealing with friction variation and enhancing the motion tracking performance of the Bowden-cable actuator system.

To handle this friction variation, some researchers have integrated fuzzy controllers or neural networks into Bowden-cable actuation systems [24], [25]. However, both approaches present certain complexities. The rules of the fuzzy controller are not standardized and rely heavily on expert experience, while determining the weights and structure of the neural network remains challenging. An alternative is the nonlinear adaptive controller proposed in [9], which estimates friction at each sampling step for accurate DC motor tracking. Its performance is sensitive to adaptation gains and initial parameter estimates. Moreover, the method lacks a clear strategy for velocity computation, and in practice, velocity measurement noise can affect stability. This control algorithm also requires a high sampling rate, which increases the computational load.

To address these challenges, twisting and super-twisting algorithms, which represent key classes of second-order sliding modes (SOSMs), are introduced for their finite-time stability and robustness against varying disturbances. These switching controllers can drive the system to zero error dynamics despite external perturbations, making them well-suited for electromechanical systems with nonlinearities such as friction and impacts [26]. Their simple structure has led to wide adoption, including applications such as orbital stabilization of bipedal robots under model uncertainties [27]. However, when using twisting controller, the chattering effect occurs in the control process due to the important switching gain [28]. For wearable robotics, this issue can further lead to poor physical human-robot interaction (pHRI) performance and low energy efficiency during tasks, which need to be considered in controller design.

Based on these considerations, a smoothed modification of the twisting controller and the super-twisting velocity observer, augmented with linear gains [26], is proposed in the controller design for Bowden-cable actuator system, which can be considered as a perturbed double-integrator model. The former modification represents a parameterized family of homogeneous continuous controllers and it is made to avoid the undesired chattering phenomenon that appears in the closed-loop system if driven by a switching input of high frequency [29]. To our knowledge, this study is the first to demonstrate the effectiveness of the proposed control synthesis through experimentation since its invention in 2010. Experimental validation demonstrates that the resulting closed-loop system is globally finite-time stable, regardless of the accumulated bending angle configuration or the nonlinear friction present in the Bowden-cable actuation system.

This letter is organized as follows: Section II presents the modeling of Bowden-cable actuator system subject to friction variation; In Section III, modified twisting controller and super-twisting velocity observer are proposed in the controller design; Following that, the control performance indices, including tracking accuracy and energy efficiency, are introduced in Section IV;

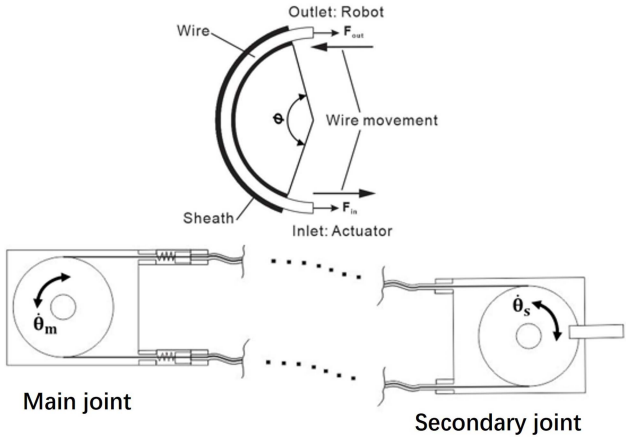

Fig. 1. Schematic representation of force and motion transmission in the studied Bowden-cable actuator system.

In Section V, experimental validation step is carried out for analyzing the control performance of the proposed control synthesis. Finally, Section VI offers conclusions and perspectives.

II. Modeling of a Bowden-Cable Actuator System

A. Friction Force of Bowden-Cable System

As the inner wire moves through the bent sheath, the friction between the wire and the sheath results in tension difference between the inlet and outlet of the wire. The widely-used theoretical model based on Coulomb friction for describing the relationship between the input and output cable-tension forces of Bowden-cable system is the Capstan formula [19]:

$$F_{out} = F_{in}\mathrm{e}^{-\mu\phi} + F_0(\mathrm{e}^{-\mu\phi} - 1) \tag{1}$$

where F_{out} and F_{in} denote the output and input cable tension force. Parameter μ denotes the kinetic friction coefficient between the sheath and the inner wire. F_0 is a tension-independent component, corresponding to the normal force that exists when the input tension F_{in} is zero [30]. As illustrated in Fig. 1, ϕ denotes the total bending angle of Bowden cable.

B. Pulley-to-Pulley Transmission System

In a Bowden-cable transmission system, a flexible sheath guides a cable, allowing remote actuation of a robotic joint by transmitting force through the relative displacement between the cable and the sheath. As shown in Fig. 1, a pulley-to-pulley configuration is considered the optimal choice for implementing a remote-actuated rotary joint, with the cables fixed on both sides of the pulleys [31]. In Fig. 1, high-stiffness compression springs are connected to the sheath for pre-tensioning the cable at various bending angles [32], generating the normal force F_0. The actuating torque τ_a at the main joint can be expressed as follows:

$$\tau_a = I_m\ddot{\theta}_m + F_{in}r_m\delta_m + f(\phi, \dot{\theta}_s) \tag{2}$$

The secondary joint dynamics can be then stated as:

$$F_{out}r_s\delta_s - I_s\ddot{\theta}_s - \tau_d = 0 \tag{3}$$

where I_m and I_s denote the moments of inertia of main and secondary joint. r_m and r_s are the radii of the main and secondary joint. $f(\phi, \dot{\theta}_s)$ represents the viscous term. θ_m and θ_s are the joint angles of the main and secondary joints, respectively. $\delta_{m,s}$ is the sign of joint velocity, which is given by

$$\delta(\dot{\theta}_{m,s}) = \begin{cases} 0 & \text{if } \dot{\theta}_{m,s} < 0 \\ 1 & \text{if } \dot{\theta}_{m,s} >= 0 \end{cases} \tag{4}$$

τ_d is the known external load applied at the secondary joint. Using the equations (1) and (3), the input rope tension F_{in} can be expressed as follows:

$$F_{in} = \frac{\left(I_s\ddot{\theta}_s + \tau_d\right) \mathrm{e}^{\mu\phi}}{r_s\delta_s} + F_0(\mathrm{e}^{\mu\phi} - 1) \tag{5}$$

This expression can then be substituted into (2) and the actuating torque is rewritten as follows:

$$\begin{aligned} \tau_a = I_m\ddot{\theta}_m + \frac{r_m\delta_m}{r_s\delta_s}\mathrm{e}^{\mu\phi}\left(I_s\ddot{\theta}_s + \tau_d\right) \\ + F_0(\mathrm{e}^{\mu\phi} - 1)r_m\delta_m + f(\phi, \dot{\theta}_s) \end{aligned} \tag{6}$$

When wearing the robot, since the frequency of human limb movement is limited (below 5 Hz) [33] and the used compression springs have high stiffness, it could be assumed that $\theta_s \approx \theta_m$; $\dot{\theta}_s \approx \dot{\theta}_m$; $\ddot{\theta}_s \approx \ddot{\theta}_m$; $\delta_m \approx \delta_s$. This hypothesis will be experimentally validated in Section V. Eq (6) can then be restated as:

$$\tau_a = I\ddot{\theta}_s + \frac{r_m}{r_s}\mathrm{e}^{\mu\phi}\tau_d + f(\phi, \dot{\theta}_s) + F_0(\mathrm{e}^{\mu\phi} - 1)r_m\delta_s \tag{7}$$

where,

$$I = I_m + \frac{r_m}{r_s}I_s\mathrm{e}^{\mu\phi} \tag{8}$$

I denotes the effective inertia of Bowden-cable transmission system. The joint acceleration of the secondary $\ddot{\theta}_s$ can be deduced from (7) such as:

$$\ddot{\theta}_s = I^{-1}\left(\tau_a - \frac{r_m}{r_s}\mathrm{e}^{\mu\phi}\tau_d - f\left(\phi, \dot{\theta}_s\right) - F_0(\mathrm{e}^{\mu\phi} - 1)r_m\delta_s\right) \tag{9}$$

Since the function f and the parameter F_0 are not well known and ϕ varies, we can consider the nominal model as follows:

$$\ddot{\theta}_s = I^{-1}\left(\tau_a - \frac{r_m}{r_s}\mathrm{e}^{\mu\phi}\tau_d\right) \tag{10}$$

Let $\ddot{\theta}_s = \ddot{\theta}_s^d + u$ be the desired behavior of the secondary joint, u being a new input control. The model-based control law τ_a becomes

$$\tau_a = I(\ddot{\theta}_s^d + u) + \frac{r_m}{r_s}\mathrm{e}^{\mu\phi}\tau_d \tag{11}$$

The state vector $\mathbf{x}$ can be defined as $\mathbf{x} = (x_1 \quad x_2)^\top = (\theta_s \quad \dot{\theta}_s)^\top$. The desired state vector is $\mathbf{x^d} = (x_1^d \quad x_2^d)^\top = (\theta_s^d \quad \dot{\theta}_s^d)^\top$. Then, the following state-space representation of the Bowden-cable actuator model (7) with (11) is obtained:

$$\dot{\mathbf{x}} = \begin{pmatrix} \dot{x}_1 \\ \dot{x}_2 \end{pmatrix} = \begin{pmatrix} x_2 \\ \dot{x}_2^d + u + w \end{pmatrix} \tag{12}$$

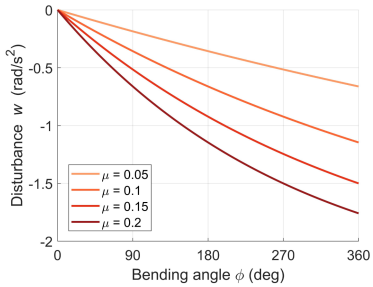

Fig. 2. The disturbance induced by the bending angle variation from 0° to 360° under different friction coefficients μ, with $F_0 = 1$ N. The simulation parameters are the same as the experimentation in Section V: $r_m = r_s = 3.2 \times 10^{-2}$ m, $I_m = 4.7 \times 10^{-5}$ kg·m^2, and $I_s = 1.3 \times 10^{-2}$ kg·m^2.

TABLE I
PERFORMANCE METRICS VALUE

	0°	90°	180°	360°
Steady-state error of Twisting (deg)	0.02	0.23	0.23	0.23
Steady-state error of PID	0.02	-0.21	0.37	-1.66
Steady-state error of adaptive controller	-0.07	1.38	1.51	2.26
Overshoot of Twisting (deg)	28.51	24.46	20.77	1.08
Overshoot of PID	28.73	26.01	25.56	24.60
Overshoot of adaptive controller	47.75	48.24	47.14	47.97
Rise time of Twisting (s)	0.10	0.11	0.12	0.13
Rise time of PID	0.05	0.06	0.06	0.06
Rise time of adaptive controller	0.05	0.05	0.052	0.054
ITAE of Twisting (deg · s)	3.52	3.27	2.84	1.70
ITAE of PID	1.22	6.62	6.28	8.27
ITAE of adaptive controller	1.60	7.30	7.84	11.19
Joule effect of Twisting (mA^2 · s)	3175	3012	2788	1917
Joule effect of PID	20492	19153	20510	18913
Joule effect of adaptive controller	19000	21353	19857	20962
Standard deviation of Super-Twisting (deg/s)	397	166	130	144
Standard deviation of Backward Difference	11967	6205	6635	2611

where,

$$w = I^{-1}\left(F_0(1 - \mathrm{e}^{\mu\phi})r_m\delta_s - f(\phi, x_2)\right)$$

w denotes the unknown external disturbances in the Bowden-cable actuator system. As shown in Fig. 2, when the viscous effect is neglected, the disturbance variation over the range $\phi = 0°$ to $360°$ increases with the friction coefficient μ. Given a Bowden-cable system, disturbance w grows exponentially as the bending angle increases, which degrades the control performance, such as steady-state error (demonstrated in Section V / Table I). Fig. 2 highlights the key role played by two of cable-driven's parameters, ϕ and μ. Particularly, the bending angle ϕ is difficult to measure. Instead of considering a global robust control, our strategy is based on the calculation of the feedback linearization control, τ_a with a reference value ϕ. And the control input u is then designed to reject the disturbance w acting on the double integrator system. In the following sections, an input-output linearizing controller is developed for the single-input and single-output (SISO) system (12) to achieve control objectives, such as tracking a reference trajectory.

III. FINITE TIME STABILIZATION OF A PERTURBED DOUBLE INTEGRATOR

A. Modified Twisting Controller

Although Coulomb friction was taken into account when modeling the Bowden-cable actuator system in Section II, there are still unknown disturbances in the dynamic system (see (12)) such as modeling errors, backlash, and other nonlinear frictional phenomena that degrade control performance in terms of both accuracy and energy efficiency.

IEEE Robotics and Automation Letters (RA-L) paper, presented at ICRA 2026, Vienna, Austria. Cite as RA-L paper.

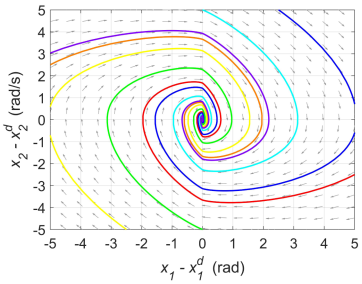

Fig. 3. Phase portrait of a double integrator model controlled by the law (13), with parameters $\lambda_1 = 1$, $\lambda_2 = 2$, and $\alpha = 0.5$, designed to drive the system towards the zero dynamics $x_2^d = x_1^d = 0$.

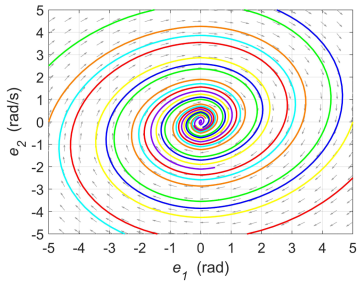

Fig. 4. Phase portrait of the second-order observation error system (17), specified with $k_1 = 0.1$, $k_2 = 0.1$, $k_3 = 0.1$, $k_4 = 1$, and $\varepsilon = 0.5$.

Many nonlinear controllers have been proposed to address external disturbances [34], including twisting algorithms which are widely recognized for their robustness properties and finite time stability [35]. The controllers, which have switching terms, are capable of forcing the dynamic system to the zero dynamics of error in spite of the external disturbances. However, in the twisting controller, chattering occurs in the dynamics system due to the important switching gain and results in low reliability of mechanical systems. The following twisting controller that incorporates a homogeneous modification [26], is proposed to achieve the finite-time orbital stabilization of the perturbed double integrator (12) around the reference trajectory $\mathbf{x^d}$, with parameters $\lambda_2 > \lambda_1 > 0$ and $\alpha \in [0,\ 1)$.

$$\begin{aligned} u = & -\lambda_1 \left|x_2 - x_2^d\right|^{\alpha} \operatorname{sign}(x_2 - x_2^d) \\ & -\lambda_2 \left|y - x_1^d\right|^{\frac{\alpha}{2-\alpha}} \operatorname{sign}(y - x_1^d) \end{aligned} \tag{13}$$

where variable y defines the measure of x_1. With $\alpha \in (0,\ 1)$, (13) is a continuous controller that helps avoid the unwanted chattering phenomenon that would accompany high-frequency switching in the closed-loop system. It represents a simplified version of the continuous controller proposed by [36].

Theorem 1: Given $\alpha \in (0, 1)$ and $\lambda_1, \lambda_2 > 0$, the continuous closed-loop system (12), (13) is globally asymptotically stable for any disturbance w, satisfying the following growth condition:

$$\|w\| \leq \lambda_0 \|x_2 - x_2^d\|^{\alpha} \tag{14}$$

for an arbitrary $\lambda_0 < \lambda_1$. The proof of this theorem driven by (13), can be found in [26]. The phase portrait of the controller is shown in Fig. 3, which illustrates its asymptotic stability when applied to a double integrator.

B. Finite Time Velocity Observer

However, it is not always easy for a mechatronic device to measure the velocity variables. This can be due to various reasons, including the need to minimize costs by reducing the number of sensors, physical limitations, or the absence of specific sensors. In such cases, an estimation of the velocity variables by software is essential. It processes the incomplete and imperfect information supplied by the available sensors, allowing the reconstruction of a dependable estimate of the entire system state.

In Bowden-cable actuator systems, a common approach calculating the velocity variables is to derive it from the measured position, such as widely used backward difference method [37]. However, the presence of noise and unknown disturbances in the control system could not be neglected. The precision of velocity estimation and the closed-loop system's stability heavily rely on the hardware performance.

The purpose of an observer is to estimate the unmeasurable states of a system based only on the measured outputs and the knowledge of the inputs. It is essentially a mathematical replica of the system. For a perturbed double-integrator model like (12), it is proposed to apply a super-twisting observer, which presents a finite time stability and robustness to uncertainties and disturbances. The form of the velocity observer is given as follows:

$$\begin{aligned} \dot{\hat{x}}_1 - \dot{x}_1^d &= \hat{x}_2 - x_2^d + k_1 |y - \hat{x}_1|^{\varepsilon} \operatorname{sign}(y - \hat{x}_1) \\ &\quad + k_2 (y - \hat{x}_1) \\ \dot{\hat{x}}_2 - \dot{x}_2^d &= u + k_3 \operatorname{sign}(y - \hat{x}_1) + k_4 (y - \hat{x}_1). \end{aligned} \tag{15}$$

where k_i, $i = 1, 2, 3, 4$ are positive parameters, and ε is such as:

$$\varepsilon \in \left[\frac{1}{2}, \frac{2}{3}\right] \quad \text{and} \quad \alpha = 1 - \varepsilon, \tag{16}$$

Subtracting (12) and (15), the observation error $e = (e_1, e_2)^{\top}$, $e_1 = x_1 - \hat{x}_1$, $e_2 = x_2 - \hat{x}_2$ is governed by the following second-order system (phase portrait shown in Fig. 4)

$$\begin{aligned} \dot{e}_1 &= e_2 - k_1 |e_1|^{\varepsilon} \operatorname{sign}(e_1) - k_2 (e_1), \\ \dot{e}_2 &= w - k_3 \operatorname{sign}(e_1) - k_4 (e_1) \end{aligned} \tag{17}$$

Substituting the x_2 velocity in (13) leads to the finite time stabilizing output feedback

$$\begin{aligned} u = & -\lambda_1 |\hat{x}_2 - x_2^d|^{\alpha} \operatorname{sign}(\hat{x}_2 - x_2^d) \\ & -\lambda_2 |y - x_1^d|^{\frac{\alpha}{2-\alpha}} \operatorname{sign}(y - x_1^d) \end{aligned} \tag{18}$$

Theorem 2: Consider system (12) under the growth condition (14) on the external disturbance w. Let (12) be driven by the observer-based dynamic feedback (15), (18) with parameters α and ε subject to (16), with positive controller gains λ_1, λ_2 such that $\lambda_1 > \lambda_0$, and with observer parameters $k_i,\ i = 1, 2, 3, 4$, satisfying the following condition:

$$\begin{aligned} k_1 > 0,\ k_2 > 1,\ k_3 > & \max\left\{\frac{\lambda_0 k_1}{k_2}, \frac{\lambda_0(\lambda_0 + k_2)}{k_1}\right\}, \\ & k_4 > \frac{\lambda_0(\lambda_0 + k_2)}{k_2}. \end{aligned} \tag{19}$$

Then the closed-loop system (12), (15), and (18) is globally asymptotically stable, regardless of whichever external disturbance (14) affects the system.

The proof of this theorem can also be found in [26].

IV. Control Performance Index

A. Tracking Accuracy Criterion

To evaluate trajectory tracking accuracy, various error indices have been proposed. Since viscous friction in Bowden-cable transmission could vary with the bending angle, the Integral of Time-weighted Absolute Error (ITAE) is preferred due to its greater sensitivity to changes in damping ratio than other metrics such as ISE [38]. This criterion minimizes the following performance index:

$$\text{ITAE} = \int_{t_0}^{t_f} t \cdot |x_1 - x_1^d| \, \mathrm{d}t \tag{20}$$

It penalizes errors that occur later in a unit-step response more heavily than initial errors, which can be used for evaluating the oscillations and steady-state accuracy of the system.

B. Energy Efficiency Criterion

Friction aside, most of the energy consumed in electric motors is due to loss by Joule effect [28], i.e. the conversion of electrical energy into heat when a current passes through resistance. To evaluate the loss E_{loss}, the following criterion is introduced for the Bowden-cable actuator system:

$$E_{loss} = \int_{t_0}^{t_f} i_a^2 \mathrm{d}t \tag{21}$$

where i_a is the actuator current. This represents the energy drawn from the battery to produce the desired motion. Joule heating also degrades the reliability of electrical components.

C. Velocity Estimation Criterion

The measurement noise in x_1 from an encoder can significantly impact the joint velocity estimation $\hat{x}_2$, leading to abrupt changes between consecutive sampling points. Therefore, to assess the quality of the estimated signal, the following standard deviation [39] is introduced:

$$\sigma = \sqrt{\frac{1}{n}\sum_{i=1}^{n}\left(\Delta\hat{x}_2(i) - \overline{\Delta\hat{x}_2}\right)^2} \tag{22}$$

where $\Delta\hat{x}_2(i) = \hat{x}_2(i) - \hat{x}_2(i-1)$ denotes the change of secondary joint velocity at the i-th sampling point; $\overline{\Delta\hat{x}_2}$ is the mean value of $\Delta\hat{x}_2$. $n = tf/h$ denotes the total number of sampling points with the sampling period h.

V. Experimental Validation

A. Experimental Setup

The prototype of Bowden-cable actuator system is shown in Fig. 5. Two 1-meter Bowden cables were manufactured by SHIMANO [40], each comprising a 1.2 mm diameter stainless steel wire and a 4 mm diameter polyethylene sheath. The length of the load arm is 0.12 m.

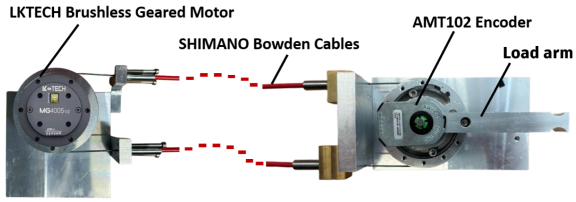

Fig. 5. The proposed prototype in the experiment uses an LKTECH brushless geared motor to actuate the main joint and an AMT102 encoder is installed at the rotational axis of secondary joint to measure its position.

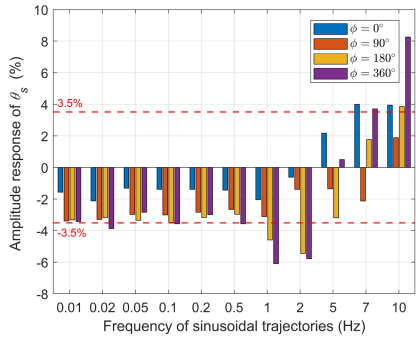

Fig. 6. Amplitude response of θ_s, as a percentage of θ_m, at the total bending angles $\phi = 0°, 90°, 180°$, and $360°$ across the discrete frequencies of sinusoidal trajectory ranging from 0.01 to 10 Hz.

In the experiment, the position control or torque control commands are transmitted from a Raspberry Pi 3B+ (Cortex-A53 64-bit SoC, running at 1.4 GHz) to a LKTECH brushless geared motor (motor type: MG4005v2, nominal torque: 1 Nm, nominal speed: 253 rpm, gear ratio: 10:1) at the main joint via CAN communication, with a sampling rate of 200 Hz. At the secondary joint, an AMT102 encoder with a resolution of 8196 CPR (counts per revolution) is employed for measuring the secondary joint position θ_s.

B. Characterization of Bowden Cable Transmission

The first step of the experiment aims at characterizing the relationship between the input main angle θ_m and the output secondary angle θ_s of a Bowden-cable actuator system. Position control commands for sinusoidal trajectories are sent to the brushless geared motor. The amplitude responses of θ_s are recorded under different bending angles ($\phi = 0°, 90°, 180°$, and $360°$) across the trajectory frequencies ranging from 0.01Hz to 10Hz, as illustrated in Fig. 6.

From the figure, it can be observed that when the bending angle of the Bowden cable is $0°$, $90°$, and $180°$, the amplitude response magnitude remains within $\pm 6\%$. Due to the elasticity of the cable, the amplitude of the output angle θ_s becomes higher than the input angle θ_m when the frequency exceeds 5 Hz. For example, the maximum amplitude response is 8%, which is observed at 10 Hz with a bending angle of $360°$. Note that in wearable robotics applications such as upper-limb exoskeleton robots, the maximum frequency of human arm movement typically remains below 5 Hz. [33] also reports that the voluntary movements of the knee joint occur at frequencies below 2 Hz. Within this lower range, most of the amplitude responses observed in the experiment fall within $\pm$ 3.5%. Thus, the hypothesis $\theta_s \approx \theta_m$ made in Section II is validated and the

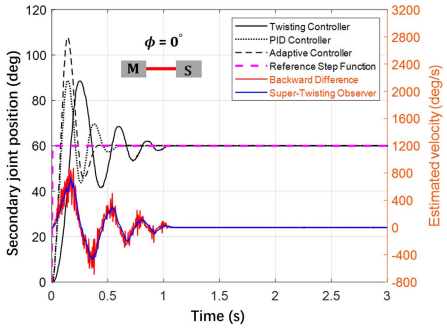

Fig. 7. Tracking the desired step trajectory $\theta_s^d = 60°$ at the total bending angle $\phi = 0°$. (the left vertical axis represents θ_s value; the right vertical axis represents the estimated $\dot{\theta}_s$ value.).

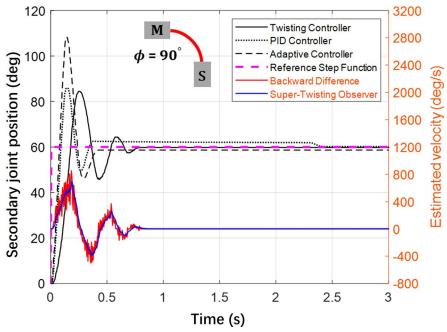

Fig. 8. Tracking the desired step trajectory $\theta_s^d = 60°$ at $\phi = 90°$.

Bowden-cable actuator system can be theoretically considered as a perturbed double-integrator model.

C. Experimentation of the Proposed Control Synthesis

The simulation results in Fig. 2 serve as the reference values for disturbance w. To satisfy the conditions (14) and (19), the control parameters are defined as: $\lambda_1 = 4$; $\lambda_2 = 40$; $k_1 = 950$; $k_2 = 60$; $k_3 = 12$; $k_4 = 3400$; $\alpha = 0.5$; $\varepsilon = 0.5$, ensuring the finite time stability at $\phi = 0°$ (Fig. 7). Parameter μ in (11) is set to 0.1, based on experimental identification. The sampling rate of control loop is set as 200 Hz ($h = 5$ ms). At each sampling step, the actuating torque τ_a is computed using (11), and the corresponding torque control command is sent to the brushless motor at the main joint via CAN communication (see Part I of the supplementary video: https://youtu.be/0UlzVSokDHE). The control performance is subsequently analyzed by varying the accumulated bending angle ϕ to 90°, 180°, and 360° (Figs. 8–10). In the experiment, the performance of the proposed controller is compared to a conventional PID controller and the friction compensation adaptive controller presented in [9].

As illustrated in Figs. 7–10, the secondary joint angle θ_s successfully converges to the reference step trajectory $\theta_s^d = 60°$ within a finite time, under various bending angle conditions. The steady-state error of all cases is below 0.4%, demonstrating that the proposed control framework effectively ensures both tracking accuracy and finite time stability. As shown in Table I, the dynamic response speed and overshoot in the control process are affected by the total bending angle. For example, the rise time at 0° (Fig. 7) is 23% shorter than at 360° (Fig. 10), while the overshoot is reduced by up to 96% at 360°.

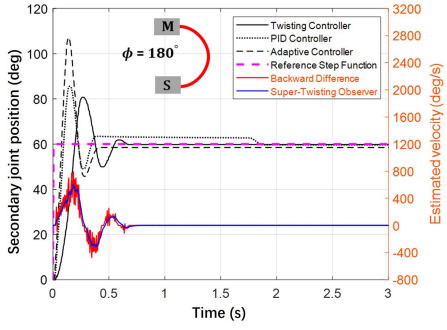

Fig. 9. Tracking the desired step trajectory $\theta_s^d = 60°$ at $\phi = 180°$.

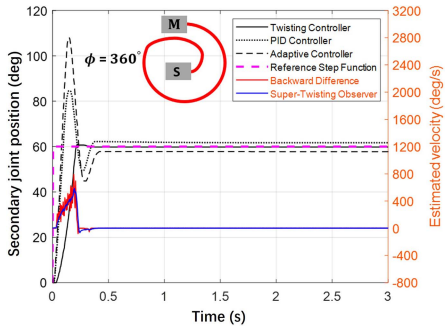

Fig. 10. Tracking the desired step trajectory $\theta_s^d = 60°$ at $\phi = 360°$.

Moreover, as the bending angle increases, the oscillations become less important, and the settling time decreases. This behavior is reflected in the ITAE criterion, which penalizes later-stage displacement errors in the control process. A longer settling time accompanied by oscillations leads to a significant increase in the ITAE value. In Table I, the ITAE for 0° is 52% higher than the minimum in the table, corresponding to the significant oscillations in the control process. Due to the weak oscillation and fast settling time, the least Joule effect occurs at 360°, which is 40% lower compared to that at 0°.

Although the angular position graphs (Figs. 7–10) may give the impression of a continuous signal, it is nonetheless a measured signal sampled at the 5 ms period. When digitally derived with the backward difference method, i.e., the simplest Euler differentiation (function of Matlab diff), we can observe noise (see red curves in Figs. 7–10). The figures clearly present that the velocity estimated by the super-twisting observer (blue curves) exhibits less noise compared to the backward difference method. It can be observed in Table I, using the super-twisting observer, the criterion value (22) has been reduced by over 94% compared to the backward difference method. This important reduction demonstrates the robustness of the proposed observer against measurement noise and provides a more reliable estimation of the secondary joint velocity in the Bowden-cable actuation system.

These experimental results reveal a clear association between the viscous effect and the accumulated bending angles of the Bowden cable: the more pronounced the bending of the sheath, the stronger the viscous effect is. To our knowledge, this study is the first to experimentally demonstrate that the sheath bending angle affects the viscous effect of Bowden-cable transmission. This effect should be taken into account when designing the controller for optimal performance. It is also important to note

that the overshoot and oscillations observed at $\phi = 0°$, $90°$, and $180°$ could be problematic when the system is coupled to a human joint in an exosuit design. To minimize these undesired phenomena, it is recommended to adjust the controller gains λ_1 and λ_2 to effectively dampen the system (see Part II of the supplementary video). However, the optimal tuning also depends on the relative placement and movement of the main and secondary joints in the application, while taking into account the viscous effect.

A comparative performance analysis with a widely-used PID controller and the adaptive controller is presented in Table I and shown in Figs. 7–10. The PID parameters ($K_p = 140$, $K_D = 4$, $K_i = 1$) are chosen for high dynamic performance, resulting in a shorter rise time than the proposed controller while maintaining similar steady-state errors. The steady-state error of the PID controller increases as ϕ varies from $0°$ to $360°$, with the error at $\phi = 360°$ reaching as much as seven times that of the proposed controller. At $\phi = 0°$ (Fig. 7), the PID controller produces less oscillation and achieves an ITAE nearly three times lower than that of the proposed controller. However, the PID controller shows significantly high ITAE values at $\phi = 90°$, $180°$, and $360°$, indicating long settling times and increased oscillations. At $\phi = 360°$, the ITAE of the PID is over six times higher than that at $0°$. The proposed controller also reduces Joule losses by over 84% compared to the PID controller.

As shown in Table I and Figs. 7–10, the adaptive controller achieves a shorter rise time and fewer oscillations than the proposed method at $\phi = 0°$, $90°$, and $180°$, using the control parameter values adopted from [9]. This controller offers advantages when the bending angle remains fixed and there are significant model uncertainties, such as variations in inertia [9]. However, at high bending angles, its performance declines, requiring parameter retuning. For example, at $\phi = 360°$, the proposed controller reduces the ITAE and Joule losses by up to 85% and 91% respectively compared to the adaptive controller. The adaptive controller is also more complex to implement as it requires the identification of eight parameters, whereas the twisting controller primarily depends on only three: λ_1, λ_2, and α. Overall, the experimental results demonstrate the effectiveness of the proposed control framework in enhancing disturbance rejection and energy efficiency under varying bending angles. Besides, the increased steady-state error and rise time at $\phi = 360°$ in Table I confirm the limitation of [23], which fixes the bending angle at $360°$ for accurate feedforward compensation, resulting in significant friction effects.

Another experiment has been conducted to track a 1 Hz sinusoidal trajectory at $\phi = 90°$ and $180°$, as commonly encountered in upper-limb exosuits. In control law (11), the reference bending angle ϕ is set as $90°$. As shown in Fig. 11, the average absolute tracking error in both cases remains within $2°$ in the no-load condition ($1.7°$ at $\phi = 90°$ and $2°$ at $\phi = 180°$). With a 0.25 Kg load applied at the end-effector, the error increases by less than $1°$ ($2.4°$ at $\phi = 90°$ and $3°$ at $\phi = 180°$) in each case (see Part III of the supplementary video). With a 0.5 Kg load, the errors in both cases increases to $3.2°$ and $4.4°$. It can be observed in Fig. 11 that the maximum time delay is less than 0.1s. Thus, these results confirm the proposed method's effectiveness in trajectory tracking and its robustness against external loading. It should be noted that the load applied at the end-effector causes axial deformation of the cable due to its elasticity [41], which affects control accuracy and will be addressed in future work.

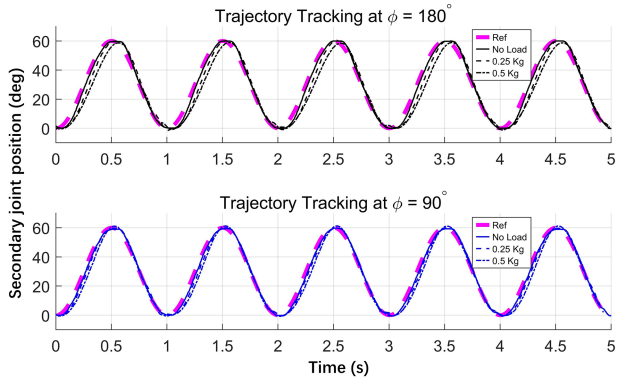

Fig. 11. Tracking a 1 Hz sinusoidal trajectory at bending angles $\phi = 180°$ and $360°$ with different load conditions, using the twisting controller. The control parameters are defined as: $\lambda_1 = 6$; $\lambda_2 = 40$; $k_1 = 600$; $k_2 = 60$; $k_3 = 12$; $k_4 = 3400$; $\alpha = 0.5$; $\varepsilon = 0.5$.

It is known that, when wearing the robot, the sheath bending angle varies continuously. Given a defined exoskeleton workspace and range of bending angles, the magnitude of external disturbances such as friction between the sheath and cable is thereby bounded. Then, the finite time stability could be achieved by selecting the control parameters that satisfies the conditions specified in (14) and (19).

VI. Conclusion

A complex mechanical mechanism for transmitting efforts, ideally suited to driving exoskeletons or other wearable assistance systems, is being studied. The mechanism consists of a main and a secondary joint linked by a Bowden-cable transmission. It is modeled and studied experimentally. Based on a super-twisting algorithm, a control law is associated with a velocity observer. Both allow convergence in finite time. This structure respects the principle of separation, i.e., the stability of the control and that of the observer guarantee the stability of the control/observer assembly. When tracking a step function, the steady-state errors remain below 0.4% across bending angles from $0°$ to $360°$. Compared to PID and the friction adaptive controller, the proposed approach achieves reductions of over 54% in ITAE and 85% in Joule energy consumption at high bending angles of $180°$ and $360°$. During sinusoidal trajectory tracking, the absolute tracking error increases by less than $1°$ as a 0.25 Kg load is added. The experimental results validate the suitability and effectiveness of the control strategy. In addition, the simplicity of the twisting controller structure also contributes to its practical applicability. However, the main limitation of this work is the lack of consideration for realistic exoskeleton usage scenarios. In particular, the effects of substantial load variations resulting from changes in arm posture or during object/tool manipulation should be thoroughly assessed and considered. The perspective for this work is to develop an effective algorithm that translates the user's motor intention into the desired actuator motion for elbow assistance, which can be accurately tracked by the proposed controller. The cable elasticity and dynamic friction model will be considered in controller design. Future evaluations will focus on the control performance when the Bowden-cable actuator system is coupled with the human elbow joint for upper-limb assistance.

REFERENCES

[1] M. P. D. Looze, T. Bosch, F. Krause, K. S. Stadler, and L. W. O'sullivan, "Exoskeletons for industrial application and their potential effects on physical work load," *Ergonomics*, vol. 59, no. 5, pp. 671–681, 2016.

[2] M. A. Gull, S. Bai, and T. Bak, "A review on design of upper limb exoskeletons," *Robotics*, vol. 9, no. 1, 2020, Art. no. 16.

[3] T. Gurriet, M. Tucker, C. Kann, G. Boeris, and A. D. Ames, "Stabilization of exoskeletons through active ankle compensation," 2019, *arXiv:1909.11848*.

[4] T. Nef and R. Riener, "ARMin-design of a novel arm rehabilitation robot," in *Proc. IEEE 9th Int. Conf. Rehabil. Robot.*, 2005, pp. 57–60.

[5] K. Kiguchi and Y. Hayashi, "An EMG-based control for an upper-limb power-assist exoskeleton robot," *IEEE Trans. Syst., Man, Cybern., Part B*, vol. 42, no. 4, pp. 1064–1071, Aug. 2012.

[6] A. Blanco, J. M. Catalán, J. A. Díez, J. V. García, E. Lobato, and N. García-Aracil, "Electromyography assessment of the assistance provided by an upper-limb exoskeleton in maintenance tasks," *Sensors*, vol. 19, no. 15, 2019, Art. no. 3391.

[7] M. A. Gull, T. Bak, and S. Bai, "Dynamic modeling of an upper limb hybrid exoskeleton for simulations of load-lifting assistance," *Proc. Inst. Mech. Engineers, Part C: J. Mech. Eng. Sci.*, vol. 236, no. 5, pp. 2147–2160, 2022.

[8] A. Ebrahimi, "Stuttgart Exo-Jacket: An exoskeleton for industrial upper body applications," in *Proc. IEEE 10th Int. Conf. Hum. Syst. Interact.*, 2017, pp. 258–263.

[9] B. K. Dinh, M. Xiloyannis, C. W. Antuvan, L. Cappello, and L. Masia, "Hierarchical cascade controller for assistance modulation in a soft wearable arm exoskeleton," *IEEE Robot. Automat. Lett.*, vol. 2, no. 3, pp. 1786–1793, Jul. 2017.

[10] Y. Lu, Y. Aoustin, and V. Arakelian, "Optimization of design parameters and improvement of human comfort conditions in an upper-limb exosuit for assistance," *Multibody Syst. Dyn.*, vol. 62, pp. 433–461, 2024.

[11] L. N. Awad et al., "A soft robotic exosuit improves walking in patients after stroke," *Sci. Transl. Med.*, vol. 9, no. 400, 2017, Art. no. eaai9084.

[12] J. Bae et al., "A lightweight and efficient portable soft exosuit for paretic ankle assistance in walking after stroke," in *Proc. IEEE Int. Conf. Robot. Automat.*, 2018, pp. 2820–2827.

[13] Q. Wang et al., "A wearable upper limb exoskeleton system and intelligent control strategy," *Biomimetics*, vol. 9, no. 3, 2024, Art. no. 129.

[14] P. Agarwal, J. Fox, Y. Yun, M. K. O'Malley, and A. D. Deshpande, "An index finger exoskeleton with series elastic actuation for rehabilitation: Design, control and performance characterization," *Int. J. Robot. Res.*, vol. 34, no. 14, pp. 1747–1772, 2015.

[15] T. Noda, T. Teramae, B. Ugurlu, and J. Morimoto, "Development of an upper limb exoskeleton powered via pneumatic electric hybrid actuators with bowden cable," in *Proc. IEEE/RSJ Int. Conf. Intell. Robots Syst.*, 2014, pp. 3573–3578.

[16] X. Li, J. Liu, W. Li, Y. Huang, and G. Zhan, "Force transmission analysis and optimization of Bowden cable on body in a flexible exoskeleton," *Appl. Bionics Biomech.*, vol. 2022, no. 1, 2022, Art. no. 5552166.

[17] D. Chen, Y. Yun, and A. D. Deshpande, "Experimental characterization of Bowden cable friction," in *Proc. IEEE Int. Conf. Robot. Automat.*, 2014, pp. 5927–5933.

[18] J. Haessig, D. A., and B. Friedland, "On the modeling and simulation of friction," *J. Dyn. Syst., Meas., Control*, vol. 113, no. 3, pp. 354–362, 1991.

[19] L. E. Carlson, B. D. Veatch, and D. D. Frey, "Efficiency of prosthetic cable and housing," *J. Prosthetics Orthotics*, vol. 7, no. 3, pp. 96–99, 1995.

[20] U. Jeong, H. In, H. Lee, B. B. Kang, and K.-J. Cho, "Investigation on the control strategy of soft wearable robotic hand with slack enabling tendon actuator," in *Proc. IEEE Int. Conf. Robot. Automat.*, 2015, pp. 5004–5009.

[21] M. Amjadi, K.-U. Kyung, I. Park, and M. Sitti, "Stretchable, skin-mountable, and wearable strain sensors and their potential applications: A review," *Adv. Funct. Mater.*, vol. 26, no. 11, pp. 1678–1698, 2016.

[22] S. Z. Homayounfar and T. L. Andrew, "Wearable sensors for monitoring human motion: A review on mechanisms, materials, and challenges," *SLAS Technol.: Transl. Life Sci. Innov.*, vol. 25, no. 1, pp. 9–24, 2020.

[23] U. Jeong and K.-J. Cho, "Feedforward friction compensation of Bowden-cable transmission via loop routing," in *Proc. IEEE/RSJ Int. Conf. Intell. Robots Syst.*, 2015, pp. 5948–5953.

[24] Q. Wu, X. Wang, B. Chen, and H. Wu, "Development of an RBFN-based neural-fuzzy adaptive control strategy for an upper limb rehabilitation exoskeleton," *Mechatronics*, vol. 53, pp. 85–94, 2018.

[25] X.-Z. Jiang, X.-H. Huang, C.-H. Xiong, R.-L. Sun, and Y.-L. Xiong, "Position control of a rehabilitation robotic joint based on neuron proportion-integral and feedforward control," *J. Comput. Nonlinear Dyn.*, vol. 7, no. 2, 2012, Art. no. 024502.

[26] Y. Orlov, Y. Aoustin, and C. Chevallereau, "Finite time stabilization of a perturbed double integrator—Part I: Continuous sliding mode-based output feedback synthesis," *IEEE Trans. Autom. Control*, vol. 56, no. 3, pp. 614–618, Mar. 2011.

[27] J. Grizzle, J.-H. Choi, H. Hammouri, and B. Morris, "On observer-based feedback stabilization of periodic orbits in bipedal locomotion," in *Proc. Methods Models Automat. Robot.*, 2007, pp. 27–30.

[28] Y. Lu, Y. Aoustin, and V. Arakelian, "Mechatronic design of dynamically decoupled manipulators based on the control performance improvement," *Robotica*, vol. 41, no. 2, pp. 609–631, 2023.

[29] Y. Aoustin, C. Chevallereau, and Y. Orlov, "Finite time stabilization of a perturbed double integrator-Part II: Applications to bipedal locomotion," in *Proc. 49th IEEE Conf. Decis. Control*, 2010, pp. 3554–3559.

[30] U. Jeong and K.-J. Cho, "Control of a Bowden-cable actuation system with embedded boasensor for soft wearable robots," *IEEE Trans. Ind. Electron.*, vol. 67, no. 9, pp. 7669–7680, Sep. 2020.

[31] A. Schiele, P. Letier, R. V. D. Linde, and F. V. D. Helm, "Bowden cable actuator for force-feedback exoskeletons," in *Proc. IEEE/RSJ Int. Conf. Intell. Robots Syst.*, 2006, pp. 3599–3604.

[32] U. A. Hofmann, T. Bützer, O. Lambercy, and R. Gassert, "Design and evaluation of a Bowden-cable-based remote actuation system for wearable robotics," *IEEE Robot. Automat. Lett.*, vol. 3, no. 3, pp. 2101–2108, Jul. 2018.

[33] G. Aguirre-Ollinger, J. E. Colgate, M. A. Peshkin, and A. Goswami, "Design of an active one-degree-of-freedom lower-limb exoskeleton with inertia compensation," *Int. J. Robot. Res.*, vol. 30, no. 4, pp. 486–499, 2011.

[34] J.-J. E. Slotine et al., *Applied Nonlinear Control*, vol. 199. Englewood Cliffs, NJ, USA: Prentice-Hall, 1991.

[35] L. Fridman and A. Levant, "Higher order sliding modes as a natural phenomenon in control theory," in *Robust Control Via Variable Structure and Lyapunov Techniques*. Berlin, Germany: Springer, 2005, pp. 107–133.

[36] S. Bhat and D. Bernstein, "Continuous finite-time stabilization of the translational and rotational double integrators," *IEEE Trans. Autom. Control*, vol. 43, no. 5, pp. 678–682, May 1998.

[37] B. Biswas, S. Chatterjee, S. Mukherjee, and S. Pal, "A discussion on euler method: A review," *Electron. J. Math. Anal. Appl.*, vol. 1, no. 2, pp. 2090–2792, 2013.

[38] K. Ogata et al. *Modern Control Engineering*. Upper Saddle River, NJ, USA: Prentice-Hall, 2009.

[39] L. Michel et al., "A semi-implicit homogeneous discretized differentiator based on two projectors: Experimental validation on a cable-driven parallel robot," *Mechan. Ind.*, vol. 25, 2024, Art. no. 11.

[40] "Shimano," Accessed: Jan. 24, 2025. [Online]. Available: https://probikeshop.fr/products/kit-de-cables-et-gaines-de-derailleur-shimano-optislik-rouge-3

[41] E. Ottaviano and G. Castelli, "A study on the effects of cable mass and elasticity in cable-based parallel manipulators," in *Proc. ROMANSY 18th Robot Des., Dyn. Control*, 2010, pp. 149–156.